Chemistry–A European Journal
Research Article
doi.org/10.1002/chem.202200559
Chemistry Europe
European Chemical Societies Publishing
www.chemeurj.org

# Olefin Metathesis Catalysts Generated In Situ from Molybdenum(VI)-Oxo Complexes by Tuning Pendant Ligands

Darryl F. Nater,[a] Christoph J. Kaul,[a] Lukas Lätsch,[a] Hayato Tsurugi,[b] Kazushi Mashima,[b] and Christophe Copéret*[a]

**Abstract:** Tailored molybdenum(VI)-oxo complexes of the form $MoOCl_2(OR)_2(OEt_2)$ catalyse olefin metathesis upon reaction with an organosilicon reducing agent at 70 °C, in the presence of olefins. While this reactivity parallels what has recently been observed for the corresponding classical heterogeneous catalysts based on supported metal oxide under similar conditions, the well-defined nature of our starting molecular systems allows us to understand the influence of structural, spectroscopic and electronic characteristics of the catalytic precursor on the initiation and catalytic proficiency of the final species. The catalytic performances of the pre-catalysts are determined by the highly electron withdrawing (σ-donation) character of alkoxide ligands, $O^tBu_{F9}$ being the best. This activity correlates with both the $^{95}Mo$ chemical shift and the reduction potential that follows the same trend: $O^tBu_{F9} > O^tBu_{F6} > O^tBu_{F3}$.

## Introduction

Olefin metathesis has become a popular reaction in organic synthesis, by enabling efficient atom economical synthetic strategies for a broad range of compounds such as pharmaceutical intermediates as well as polymers and petrochemicals.[1–5] One of the historical and noteworthy examples is the Shell Higher Olefin Process (SHOP), that is used to obtain long chains α-olefins from ethylene through olefin oligomerization and ethenolysis.[2,3,6] This process is based on supported Mo oxide olefin metathesis catalysts. While metathesis with group 6 metals such as these are proposed to involve high oxidation state metal oxo alkylidenes as active species, the mechanism of formation of these species remains unknown despite decades of intense studies (Scheme 1a).[6–8] Recent investigations, based on well-defined supported M-oxo (M = Mo, W) moieties prepared via surface organometallic chemistry, have shown that initiation is best described as involving first a reduction of M(VI) to M(IV) species that convert in the presence of olefins to M(VI) alkylidenes.[6,9–15] The involvement of these high-oxidation state Mo(VI) alkylidenes parallels what is proposed in molecular chemistry: in fact, all efficient Mo-based catalysts are based on well-defined Mo(VI) oxo or imido alkylidenes, the so-called Schrock metathesis catalysts, which have the same general formula, (X)(Y)Mo(E)(=CHR) with E = oxo or imido and X,Y = anionic ligands. Metathesis from these systems initiates rapidly through cross-metathesis of the starting alkylidene (usually a neopentylidene (R = $^t$Bu), neophylidene (R = $CMe_2Ph$) or, more recently, adamantylidene) and the olefin substrate.[16–21] These catalysts display very high turnover frequencies (TOFs) and turnover numbers (TONs) when the right ligand set is chosen, with often even higher activities upon immobilization on an oxide support.[17,19,22,23] Detailed studies have shown that, even

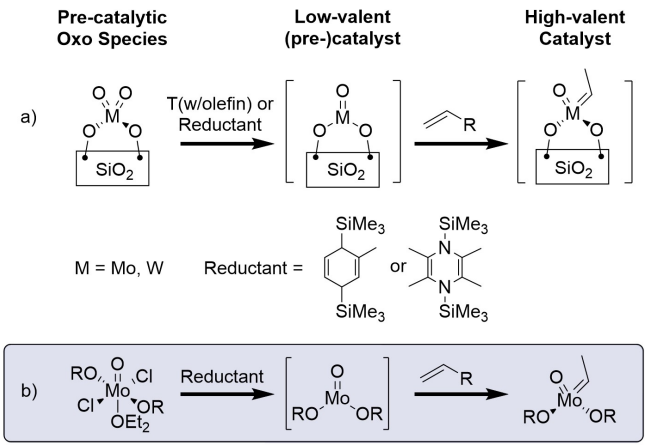


**Scheme 1.** Initiation in supported group 6 oxide-based metathesis catalysts (a), and in situ activation of high-valent molecular species (b, this work).

[a] D. F. Nater,+ C. J. Kaul,+ L. Lätsch, C. Copéret
Department of Chemistry and Applied Biosciences
ETH Zürich
Vladimir-Prelog-Weg 1–5, 8093 Zürich (Switzerland)
E-mail: ccoperet@ethz.ch

[b] H. Tsurugi, K. Mashima
Department of Chemistry
Graduate School of Engineering Science
Osaka University
1-3, Machikaneyama-cho, Toyonaka, Osaka, 560-8531 (Japan)

Supporting information for this article is available on the WWW under https://doi.org/10.1002/chem.202200559

with well-defined high oxidation state alkylidenes, low valent Mo(IV) olefin complexes or dimeric compounds are generated during metathesis;[24,25] these have been shown to display poor albeit measurable activity. In view of the given parallel between homogeneous and heterogeneous metathesis processes, one may wonder whether low valent Mo(IV) oxo compounds can initiate metathesis or not.

Building on these results, we therefore decided to investigate a method to generate low valent Mo(IV) oxo species *in-situ* from stable and well-defined Mo(VI) oxo with a wider variety of alkoxide ligands, in order to subsequently initiate metathesis in solution and to establish structure-activity relationships on these systems. We therefore decided to generate these putative species *in-situ* (in the presence of an olefin) from a series of compounds of the form $MoOCl_2(OC(CH_3)_{3-x}(CF_3)_x)_2(Et_2O)$ (**1**) combined with a molecularly-defined reducing agent (Scheme 1b). We opted for the family of compounds $\mathbf{1_{Fx}}$ (x = 3, 6 and 9) because they contain two Cl ligands that are amiable to be removed upon reduction with organosilicon reducing agent,[26] thus generating low valent and low coordinate Mo(IV) species while also giving us an opportunity to evaluate the influence of the anionic $OR_{Fx}$ ligand(s) on the formation of alkylidene.[19]

## Results and Discussion

### Synthesis of Mo(VI)-oxo complexes

The series of Mo(VI)-oxo complexes $MoOCl_2(OR)_2(Et_2O)$ ($\mathbf{1_{F3}}$: R = $CMe_2CF_3 = {}^tBu_{F3}$, $\mathbf{1_{F6}}$: R = $CMe(CF_3)_2 = {}^tBu_{F6}$, $\mathbf{1_{F9}}$: R = $C(CF_3)_3 = {}^tBu_{F9}$) was synthesized via salt metathesis of $MoOCl_4$ with 2 equiv. of the corresponding lithium alkoxide in diethyl ether at low temperatures (Figure 1). After evaporation of the solvent *in vacuo*, extraction with pentane and crystallization at −40 °C, the pure products were obtained as yellow to orange crystals, with yields varying from 20% up to 70% for the individual complexes, with $\mathbf{1_{F3}}$ having the highest yield and $\mathbf{1_{F9}}$ being obtained in the smallest quantities. Generating $\mathbf{1_{F0}}$ has so far not been possible via this approach, due to the immediate decomposition of the compound with concomitant formation of isobutene.

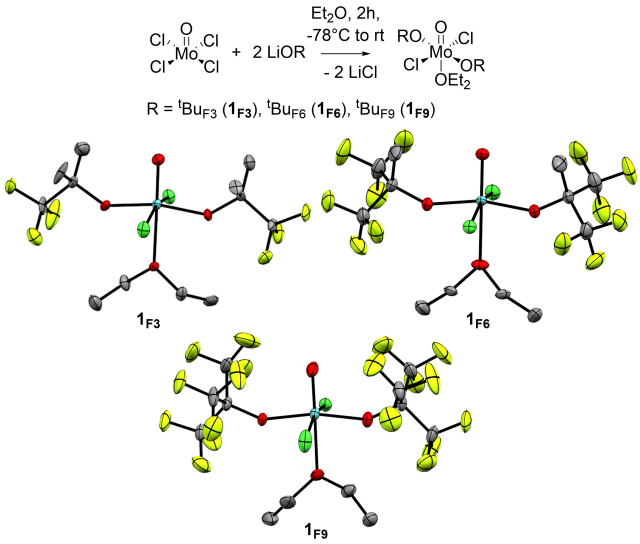


**Figure 1.** Synthetic procedures and X-ray structures of complexes $\mathbf{1_{F3}}$, $\mathbf{1_{F6}}$ and $\mathbf{1_{F9}}$. Selected bond lengths in Å ($\mathbf{1_{F3}}$/$\mathbf{1_{F6}}$/$\mathbf{1_{F9}}$): Mo=O: 1.669/1.658/1.656; Mo-OR: 1.873/1.878/1.913; Mo–Cl: 2.367/2.343/2.321; Mo-$OEt_2$: 2.300/2.283/2.277.

In all cases, these compounds display a distorted octahedral geometry with the molybdenum center slightly contorted towards the oxo ligand. The structural similarities within this series of complexes enabled us to quantitatively assess the influence of the alkoxide ligands on the complex structure and bond length.

For instance, the Mo=O bond length contracts from the complex with the least electron withdrawing alkoxide ($\mathbf{1_{F3}}$) to the most electron withdrawing perfluorinated *tert*-butyl alkoxide ($\mathbf{1_{F9}}$) from 1.669 Å to 1.656 Å. Simultaneously, a contraction of the Mo-$OEt_2$ bond from 2.300 Å to 2.277 Å is observed. These contractions are accompanied by a shortening of the Mo–Cl bond from 2.367 Å to 2.321 Å with the decrease in σ-donation from $O^tBu_{F3}$ to $O^tBu_{F9}$. Conversely, the Mo-OR bond is elongated within the series of complexes from 1.873 Å to 1.913 Å (see Table 2). These observations are also found in computed structures (B3LYP, SDD//TZVP, GD3 empirical dispersion, SMD solvation model), clearly showing that the observed structural changes are not due to specific interaction in the solid state but relate to the electronics of the species.

### Evaluation of catalytic performances

The metathesis activity of these molecular precursors was then evaluated at 70 °C in the presence of different organosilicon reducing agents (**2** or **3**) using 1-nonene and *cis*-4-nonene as prototypical substrates (Scheme 2 and Table 1).[27] Using lower temperature, for example 30 °C, leads to low catalytic activity (see Table 1), and no activity was observed in the absence of reducing agent. While reduction with both 1,4-bis(trimethylsilyl)-2-methyl-1,4-cyclohexadiene (**2**) or 2,3,5,6-tetramethyl-1,4-bis(trimethylsilyl)-1,4-diaza-2,5-cyclohexadiene (**3**) initiates metathesis, we focus on catalysis using **2**, as it proved to be vastly superior under the employed conditions (detailed kinetic

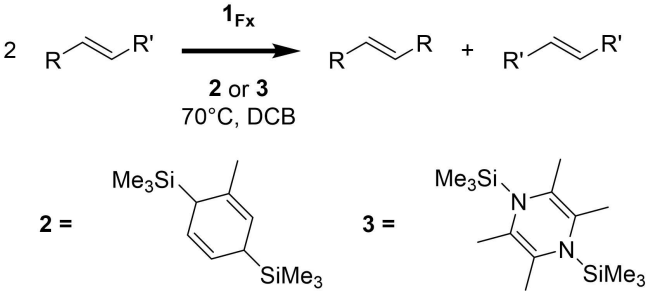


**Scheme 2.** Schematic representation of a catalytic test.

**Table 1.** Catalytic activity of complexes $\mathbf{1}_{F3}$, $\mathbf{1}_{F6}$ and $\mathbf{1}_{F9}$ following reduction with **2**. For TOFs, the corresponding conversion is given in parentheses.

| Catalytic precursor | Loading [mol %] | Substrate | $TOF_{3min}$ (30 °C) | Conversion after 24 h (30 °C) | $TOF_{3min}$ (70 °C) | Conversion after 24 h (70 °C) |
|---|---|---|---|---|---|---|
| $\mathbf{1}_{F3}$ | 0.2 | 1-nonene | 0.0 (0.0 %) | 0.0 % | 0.0 (0.0 %) | 0.5 % |
| $\mathbf{1}_{F6}$ | 0.2 | 1-nonene | 0.3 (0.2 %) | 3.2 % | 0.8 (0.5 %) | 40.9 % |
| $\mathbf{1}_{F9}$ | 0.2 | 1-nonene | 1.6 (1.0 %) | 67.1 % | 9.4 (6.0 %) | 100.0 %[a] |
| $\mathbf{1}_{F9}$ | 0.1 | 1-nonene | 0.5 (0.2 %) | 37.8 % | 11.4 (3.7 %) | 55.7 %[b] |
| $\mathbf{1}_{F9}$ | 0.2 | *cis*-4-nonene | – | – | 21.8 (12.6 %) | 45.4 %[c] |

[a] Equilibrium conversion, reached after 4 h. [b] Maximum conversion, reached after 8 h. [c] Equilibrium conversion, reached after 1 h.

and selectivity profiles and activity data are displayed in the Supporting Information).

Using **2** as reductant and 1-nonene as substrate at 70 °C, the initial turn over frequency at 3 min ($TOF_{3min}$) are ca. $<0.1$ $min^{-1}$, 0.8 $min^{-1}$ and 9.4 $min^{-1}$ for $\mathbf{1}_{F3}$, $\mathbf{1}_{F6}$ and $\mathbf{1}_{F9}$, respectively.

Given these initial rates, $\mathbf{1}_{F9}$ is the only species able to reach equilibrium conversion ($TON_{max}$ of 500) within 24 h, with $\mathbf{1}_{F6}$ and $\mathbf{1}_{F3}$ reaching ca. 41 % (TON = 174) and 0.5 % (TON = 2), respectively. Note that with $\mathbf{1}_{F9}$ the TOFs slightly increase at 10 min reaching a $TOF_{max}$ of 13.9 $min^{-1}$. Notably the corresponding well-defined alkylidene with a similar ligand set ($MoO(OtBu_{F9})_2(=CHR)$ shows a TOF of 216 $min^{-1}$ under similar conditions, albeit with a rapid decomposition. Comparing their TOF indicates that the amounts of active sites generated in situ from $\mathbf{1}_{F9}$ is probably approx. 5 %. Note that similar activities (210 $min^{-1}$) and much higher conversions are reached with $MoO(OtBu_{F9})_2(=CHR)$ at room temperature, indicating that deactivation is quite fast at 70 °C. We note that the use of a stronger reducing agent (**3**) leads to a decrease in activity (see Supporting Information). However, this decrease may also be due to the release of tetramethylpyrazine, which is formed as a side product when using **3**, as it can also be a poison for the catalytic performance. With *cis*-4-nonene as a substrate, $\mathbf{1}_{F9}$ in combination with **2** metathesis occurs with a fast initial $TOF_{3min}$ of 21.8 $min^{-1}$ and reaches maximum conversion already after one hour. We can again compare this with the TOF of the corresponding well-defined alkylidene (TOF = 177 $min^{-1}$) to determine the amounts of active species formed. This comparison suggests the formation of ~13 % active sites.

We subsequently set out to rationalize this reactivity trend using electrochemistry, titration studies and $^{95}$Mo NMR spectroscopy as these methods should provide information about redox processes[28] and electronic structures.[29]

We first investigated changes in redox behavior as a function of fluorination of the alkoxide ligands using cyclic voltammetry measurements (Figure 2). The general characteristics of the cyclic voltammogram were consistent within the Mo(VI) complex series, featuring a first reduction to Mo(V) at rather high potentials between −0.1 V and 0.7 V vs. $Fc/Fc^+$. This feature was found to be fully reversible under the investigated conditions (see Supporting Information). A second wave was observed at the lower potentials of −1.6 V to −2.1 V vs. $Fc/Fc^+$ corresponding to the reduction of Mo(V) to Mo(IV) and was found to be irreversible, likely due to a structural change induced by this reduction, presumably the loss of a chloride ligand and additional steps. Noteworthy the peak potentials directly correlate with the σ-donating ability of the

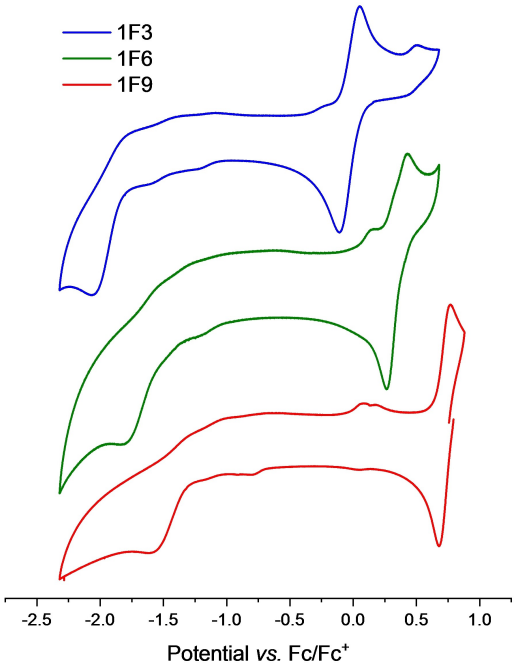


**Figure 2.** Cyclic voltammograms of $\mathbf{1}_{F3}$, $\mathbf{1}_{F6}$ and $\mathbf{1}_{F9}$ (1 mM complex in MeCN, 0.1 M $TBAPF_6$, GC working electrode, Pt counter electrode, 100 mV/s).

alkoxide ligands: the feature corresponding to the Mo(VI) to Mo(V) transition increased from −0.124 V to 0.677 V vs. $Fc/Fc^+$, between $\mathbf{1}_{F3}$ and the more electron withdrawing $\mathbf{1}_{F9}$. Likewise the reduction potential corresponding to the Mo(V)/Mo(IV) transition displayed an increase from −2.064 V to −1.599 V vs. $Fc/Fc^+$. As such, the results of the electrochemical investigation show that fluorination of the alkoxide ligand increases the redox potential or in other words decreases the energy of low-lying unoccupied molecular orbitals, allowing them to more easily accept electrons.

We also investigated the initial reduction step by $^1$H NMR. In all cases, contacting $\mathbf{1}_{Fx}$ with 2 equiv. of reducing agent (**2**) led to a full conversion of the starting material with the concomitant formation of 2 equiv. of $Me_3SiCl$, consistent with a two-electron reduction of $\mathbf{1}_{Fx}$, indicating that the initiation efficiency is likely not due to a difference of reduction efficiency but to formation of the active species from the *in-situ* generated low valent species.

Subsequently, we investigated the three compounds $\mathbf{1}_{F3\text{-}9}$ using solution $^{95}$Mo NMR in order to obtain further insight into the electronic structure of these compounds.[29,30] Here, the $^{95}$Mo chemical shift revealed a high sensitivity to subtle changes of the coordination sphere (see Table 2): The general trend is, that more

**Table 2.** Summarized characterization of complexes $\mathbf{1}_{F3}$, $\mathbf{1}_{F6}$ and $\mathbf{1}_{F9}$.

| Complex | Average bond length [Å] XRD (DFT optimization in solution) | | | | $E_{p,c}$ [V] | $E_{p,c}$ [V] | $^{95}$Mo NMR shift |
|---|---|---|---|---|---|---|---|
| | Mo=O | Mo–OR | Mo–Cl | Mo–$OEt_2$ | Mo(VI)/Mo(V) | Mo(V)/Mo(IV) | (ppm) |
| $\mathbf{1}_{F3}$ | 1.669 (1.689) | 1.873 (1.897) | 2.367 (2.403) | 2.300 (2.350) | −0.124 | −2.064 | 61 |
| $\mathbf{1}_{F6}$ | 1.658 (1.683) | 1.878 (1.915) | 2.343 (2.376) | 2.283 (2.358) | 0.264 | −1.811 | 100 |
| $\mathbf{1}_{F9}$ | 1.656 (1.675) | 1.913 (1.952) | 2.321 (2.349) | 2.277 (2.359) | 0.677 | −1.599 | 149 |

electron withdrawing alkoxide groups result in a higher chemical shift and deshielding of the nucleus with $\mathbf{1}_{F3}$ being the most shielded at $\delta_{Mo}$ = 61 ppm, $\mathbf{1}_{F6}$ showing an intermediate chemical shift of $\delta_{Mo}$ = 100 ppm and $\mathbf{1}_{F9}$ being the most deshielded at $\delta_{Mo}$ = 149 ppm.

To study the origin of the observed chemical shift trend, we calculated and analyzed the individual principal components of the chemical shift tensors.[30,31] The calculated chemical shifts agree well with experiments and the associated principal component of the CS tensors show that the $\delta_{11}$ component, which extends along the RO–Mo–OR axis (Figure 3a), drives the change in chemical shift. This component is oriented perpendicular to the Mo=O and Mo–Cl bonds and is thus associated with the magnetic couplings between either or both of these two bonds.[32]

In order to better understand the origin of this deshielding, we performed natural chemical shift analysis on two simpler model compounds, as such analysis was only possible for smaller systems: $MoO(OCH_3)_2Cl_2(Et_2O)$ and $MoO(OCF_3)_2Cl_2(Et_2O)$. This analysis shows that the diamagnetic contribution (mostly associated with core electrons) is almost identical for the two model compounds, while the paramagnetic component of the shielding changes significantly with the introduction of fluorinated ligands (Figure 3). Paramagnetic deshielding originates from couplings between frontier molecular orbitals and occurs when an occupied orbital can couple with an empty orbital of the right symmetry (orthogonal to each other and to the applied magnetic field) and close in energy.[30] By deconvoluting the contributions to $\delta_{11}$ or the related chemical shielding $\sigma_{11}$, we find that the contribution of the Mo–Cl bonding and antibonding orbitals changes only marginally and the main contribution to the change in $\sigma_{11}$, and by extension $\delta_{11}$, comes from the Mo=O bond, more specifically from the π-bonding orbitals. The Mo=O π-bond consists of the Mo=O $\pi_x$ and Mo=O $\pi_y$ orbitals, which extends along the RO–Mo–OR axis and along the axis Cl–Mo–Cl, respectively. NCS analysis shows a significant increase in deshielding only for Mo=O $\pi_y$, whereas a small increase in shielding is observed for Mo=O $\pi_x$ for the fluorinated analogue. Symmetry considerations suggest that the respective magnetic couplings are with the $\sigma^*_{Mo\text{-}OEt2}$ for the Mo=O $\pi_y$ and with the $d_{xy}$ orbital for the Mo=O $\pi_x$, respectively (Figure 3). Ligand fluorination hence lowers the energy of the $\sigma^*_{Mo\text{-}OEt2}$ (as evidenced by modulation of the Mo–$OEt_2$ bond lengths) leading to an overall increased deshielding. The increased shielding originating from the Mo=O $\pi_x$ orbital can be rationalized through the increasing strength of the π-bond with the alkoxide ligands upon fluorination (as evidenced by the respective bond angles) that raises the energy of the $d_{xy}$.

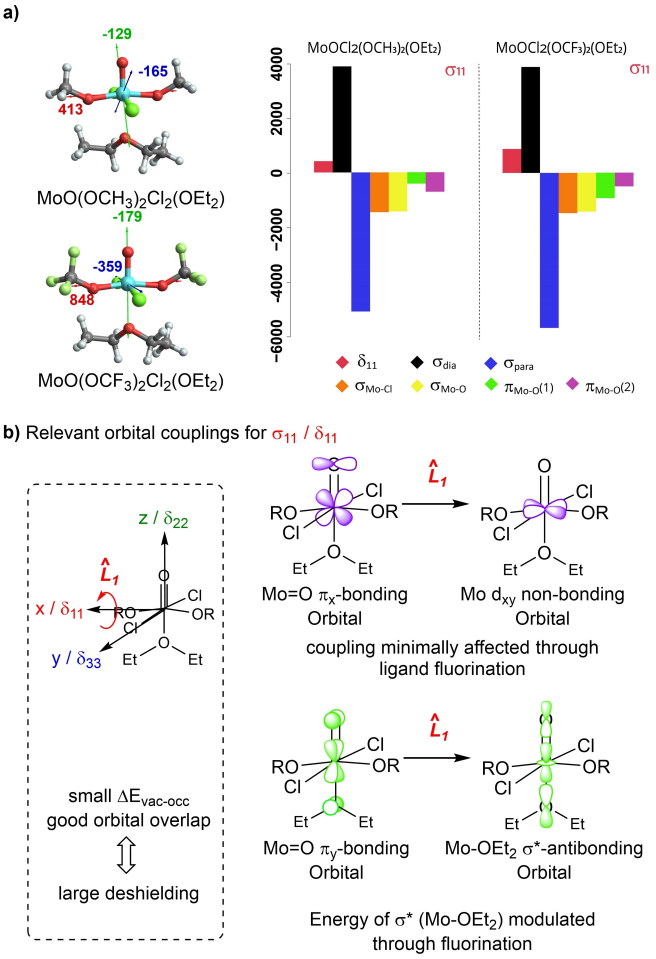


**Figure 3.** a) Contributions to the chemical shift and b) relevant orbital couplings for $\sigma_{11}$ ($\delta_{11}$) in compounds of the form $MoO(OR)_2Cl_2(OEt_2)$.

The correlation between reduction potential and $^{95}$Mo NMR chemical shift, and these parameters with the catalytic performance of this series of Mo(VI) pre-catalysts indicate that the fluoroalkoxy ligands manipulate the energy of $\sigma^*_{Mo\text{-}OEt2}$, as evidenced by NCS calculations, as well as the energy of the LUMO, which directs the reduction potentials of these Mo complexes. This decrease in orbital energy, appears to correlate with the initiation efficiency, and, by extension, the overall catalytic performance of the precatalytic compounds. Overall, both $^{95}$Mo and the redox potential could be thus noteworthy descriptors to assess the quality of pre-catalysts.

## Conclusion

We have described the synthesis and characterization of a series of high-valent molybdenum(VI)-oxo compounds, which were characterized by X-ray diffraction, cyclic voltammetry and $^{95}$Mo NMR. Due to the structural similarities of the compounds, we could correlate both structural and electronic changes with the influence of the fluorinated alkoxide ligands, showing that the reduction potential increases with an increasing degree of fluorination of the *tert*-butoxide groups, while simultaneously decreasing the shielding of the nucleus in $^{95}$Mo NMR. Both of which are due to lowered energies of metal centered orbitals. These series of Mo(VI)-oxo compounds are shown to generate olefin metathesis catalytic active species upon reaction with an organosilicon reductant in the presence of olefins. The activity trend follows the σ-donation ability of the alkoxide ligand: $\mathbf{1}_{F9} > \mathbf{1}_{F6} \gg \mathbf{1}_{F3}$ with a TOF reaching up to 13.9 min$^{-1}$ for the most active catalytic precursor $\mathbf{1}_{F9}$. Comparing with the corresponding well-defined alkylidene shows that ca. 5–15% of the initial precursor is converted into alkylidenes, depending on the olefins. It is noteworthy that the reactivity patterns follow the same trends as the redox potential and $^{95}$Mo NMR chemical shift, showing that these parameters can be used as potential descriptors of reactivity. Overall, having more electron withdrawing groups (weaker σ-donating ligands) leads to having more easily reducible molybdenum centers, that correlates with increase catalytic performance. This is likely due to a combination of factors: i) the formation of more reactive alkylidenes and ii) a higher initiation efficiency. We are currently further exploring redox potential and NMR shifts as descriptors of catalyst performances in various catalysts.

The data that support the findings of this study are available from the corresponding author upon reasonable request.

All Crystal Structures have been deposited on the Cambridge Crystallographic Structural Database with Deposition Numbers 2142651 (for $\mathbf{1}_{F3}$), 2142652 (for $\mathbf{1}_{F6}$), 2142655 (for $\mathbf{1}_{F9}$) containing the supplementary crystallographic data for this paper. These data are provided free of charge by the joint Cambridge Crystallographic Data Centre and Fachinformationszentrum Karlsruhe Access Structures service.

## *Acknowledgements*

D. N. thanks the Swiss National Science Foundation (SNSF fond number 20021 169134 and 200020B 192050). L. L. thanks the Scholarship Fund of the Swiss Chemical Industry for support. This work was partially supported by the International Joint Research Promotion Program of Osaka University. We thank Dr. Z. Berkson for help with $^{95}$Mo NMR measurements. Open access funding provided by Eidgenössische Technische Hochschule Zürich.

## Conflict of Interest

The authors declare no conflict of interest.

**Keywords:** cyclic voltammetry · fluorinated alkoxides · in situ activation · molybdenum · olefin metathesis · $^{95}$Mo NMR spectroscopy

[1] A. G. Wenzel, D. J. O'Leary, E. Khosravi, R. H. Grubbs, *Handbook of Metathesis*, Wiley-VCH Verlag GmbH & Co. KGaA, Weinheim, Germany, **2015**.
[2] J. Mol, *J. Mol. Catal. A* **2004**, *213*, 39–45.
[3] M. Schuster, S. Blechert, *Angew. Chem. Int. Ed.* **1997**, *36*, 2036–2056; *Angew. Chem.* **1997**, *109*, 2124–2144.
[4] C. S. Higman, J. A. M. Lummiss, D. E. Fogg, *Angew. Chem. Int. Ed.* **2016**, *55*, 3552–3565; *Angew. Chem.* **2016**, *128*, 3612–3626.
[5] A. H. Hoveyda, S. J. Malcolmson, S. J. Meek, A. R. Zhugralin, *Angew. Chem. Int. Ed.* **2010**, *49*, 34–44; *Angew. Chem.* **2010**, *122*, 38–49.
[6] K. Yamamoto, K. W. Chan, V. Mougel, H. Nagae, H. Tsurugi, O. v. Safonova, K. Mashima, C. Copéret, *Chem. Commun.* **2018**, *54*, 2–5.
[7] A. Chakrabarti, I. E. Wachs, *J. Phys. Chem. C* **2019**, *123*, 12367–12375.
[8] E. L. Lee, I. E. Wachs, *J. Phys. Chem. C* **2007**, *111*, 14410–14425.
[9] V. Mougel, K.-W. Chan, G. Siddiqi, K. Kawakita, H. Nagae, H. Tsurugi, K. Mashima, O. Safonova, C. Copéret, *ACS Cent. Sci.* **2016**, *2*, 569–576.
[10] Y. Iwasawa, H. Hamamura, *J. Chem. Soc. Chem. Commun.* **1983**, 130–132.
[11] Y. Iwasawa, H. Kubo, H. Hamamura, *J. Mol. Catal.* **1985**, *28*, 191–208.
[12] R. R. Schrock, C. Copéret, *Organometallics* **2017**, *36*, 1884–1892.
[13] K. Amakawa, S. Wrabetz, J. Kröhnert, G. Tzolova-Müller, R. Schlögl, A. Trunschke, *J. Am. Chem. Soc.* **2012**, *134*, 11462–11473.
[14] A. N. Startsev, B. Bogdanovic`, H. Bönnemann, V. N. Rodin, Y. I. Yermakov, *J. Chem. Soc. Chem. Commun.* **1986**, *5*, 381–382.
[15] R. R. Schrock, M. Duval-Lungulescu, W. C. P. Tsang, A. H. Hoveyda, *J. Am. Chem. Soc.* **2004**, *126*, 1948–1949.
[16] P. A. Zhizhko, F. Toth, C. P. Gordon, W. Chan, W. Liao, V. Mougel, C. Copéret, *Helv. Chim. Acta* **2019**, *102*, e1900190.
[17] V. Mougel, C. B. Santiago, P. A. Zhizhko, E. N. Bess, J. Varga, G. Frater, M. S. Sigman, C. Copéret, *J. Am. Chem. Soc.* **2015**, *137*, 6699–6704.
[18] B. Paul, R. R. Schrock, C. Tsay, *Organometallics* **2021**, *40*, 463–466.
[19] J. de Jesus Silva, M. Pucino, F. Zhai, D. Mance, Z. J. Berkson, D. F. Nater, A. H. Hoveyda, C. Copéret, R. R. Schrock, *Inorg. Chem.* **2021**, *60*, 6875–6880.
[20] M. Pucino, M. Inoue, C. P. Gordon, R. Schowner, L. Stöhr, S. Sen, C. Hegedüs, E. Robé, F. Tóth, M. R. Buchmeiser, C. Copéret, *Angew. Chem. Int. Ed.* **2018**, *57*, 14566–14569; *Angew. Chem.* **2018**, *130*, 14774–14777.
[21] D. F. Nater, B. Paul, L. Lätsch, R. R. Schrock, C. Copéret, *Helv. Chim. Acta* **2021**, *104*, e2100151.
[22] J. de Jesus Silva, D. Mance, M. Pucino, M. J. Benedikter, I. Elser, M. R. Buchmeiser, C. Copéret, *Helv. Chim. Acta* **2020**, *103*, e2000161.
[23] V. Mougel, C. Copéret, *Chem. Sci.* **2014**, *5*, 2475–2481.
[24] R. R. Schrock, J. S. Murdzek, G. C. Bazan, J. Robbins, M. Dimare, M. O. Regan, *J. Am. Chem. Soc.* **1990**, *112*, 3875–3886.
[25] J. Robbins, G. C. Bazan, J. S. Murdzek, M. B. O'Regan, R. R. Schrock, *Organometallics* **1991**, *10*, 2902–2907.
[26] H. Tsurugi, K. Mashima, *Acc. Chem. Res.* **2019**, *52*, 769–779.
[27] P. A. Zhizhko, V. Mougel, J. de Jesus Silva, C. Copéret, *Helv. Chim. Acta* **2018**, *101*, 2–7.
[28] F. W. Nyasulu, J. M. Mayer, *J. Electroanal. Chem.* **1995**, *392*, 35–42.
[29] J. A. Brito, H. Teruel, S. Massou, M. Gómez, *Magn. Reson. Biol.* **2009**, *47*, 573–577.
[30] C. P. Gordon, L. Lätsch, C. Copéret, *J. Phys. Chem. Lett.* **2021**, *12*, 2072–2085.
[31] L. Lätsch, E. Lam, C. Copéret, *Chem. Sci.* **2020**, *11*, 6724–6735.
[32] C. M. Widdifield, R. W. Schurko, *Conc. Magn. Res. A* **2009**, *34*, 91–123.

Manuscript received: February 21, 2022
Accepted manuscript online: March 2, 2022
Version of record online: March 10, 2022